Photonic generation of microwave arbitrary waveforms using stimulated Brillouin scattering and Sagnac loop*

LI Xiang (李想), **DU Cong** (都聪), **LIU Fangming** (刘芳铭), **ZHANG Zhenguo** (张振国), **and DONG Wei** (董玮)**

State Key Laboratory on Integrated Optoelectronics, College of Electronic Science and Engineering, Jilin University, Changchun 130012, China

(Received 14 October 2020; Revised 30 December 2020)

A photonic approach is proposed to generate microwave arbitrary waveforms based on the stimulated Brillouin scattering (SBS) effect and the Sagnac loop. The Sagnac loop is utilized to generate the optical signals of ±1st-order and ±3rd-order sidebands. Due to the principle of velocity adaptation, even order optical sidebands are suppressed. Thanks to the SBS effect, the microwave signal consisting of odd order harmonics is generated after the photodetector (PD), which can construct the triangular waveform, the square waveform, or the sawtooth waveform by adjusting the weight of the harmonics.

Document code: A **Article ID:** 1673-1905(2021)06-0379-6

DOI https://doi.org/10.1007/s11801-021-0155-x

In recent years, the generation of arbitrary waveforms has been attractive in microwave photonics. Arbitrary waveform microwave pulses are widely used in data communication, radio frequency (RF) communication system[1,2] and electronic devices for testing and measurement of the optical signal[3,4]. There are many methods to generate arbitrary waveforms, such as space-to-time (STT) pulse shaping method[5,6] and frequency-to-time mapping (FTTM) technique[7]. High-speed photoconverter and free-space optical components can be used in STT pulse shaping method. In that scheme, the dimension of the system is large, and additional components may create much noise so that it would lead to enormous optical power loss. At the same time, the FTTM method has disadvantages of high cost, and the low duty cycle (<1). After continuous research, the arbitrary microwave waveform could be generated by frequency comb generation and optical spectrum manipulation[8]. But in this system external modulation could increase the complexity of operation. In Ref.[9], an arbitrary microwave waveform is generated by allowing an ultra-short microwave pulse to pass through a microwave photonic filter (MPF) and a time reversal module (TRM). Due to using different optical filters to generate different waveforms, the stability of the system is limited. In Ref.[10], a dual-parallel Mach-Zehnder modulator (DP-MZM) was used to generate arbitrary waveforms. The flaw in this approach is that the ideal the repetition rate of the different waveforms is hard to be manipulated in practical applications. Then, the authors generate a microwave waveform based on two dual-drive Mach-Zehnder modulators (DD-MZMs)[11]. By utilizing a fiber Bragg grating (FBG) to remove the unideal sidebands, a triangular waveform is obtained which can't be transformed to other waveforms. In Ref.[12], a scheme using parallel-connecting high-birefringence fiber loop mirrors (Hi-Bi-FLMs) to generate a microwave waveform has been proposed. But the extinction ratios (*ERs*) of some specific spectra (square waveform and sawtooth waveform) are relatively low. In addition, generating arbitrary waveform also can use the polarization division multiplexing Mach-Zehnder modulator (PDM-MZM)[13]. Though the structure of the system is simple, it's difficult to manipulate the polarization state.

In this paper, we present a modified approach based on stimulated Brillouin scattering (SBS) effect and Sagnac loop[14-17] to generate three types of microwave waveform. Through the photodetector (PD), the microwave signal consisting of odd order harmonics is generated, which can construct the triangular waveform, the square waveform, or the sawtooth waveform. The theoretical analysis is presented, which is validated by a simulation experiment. The proposed method not only improves the stability of the system, but also has the potential in full optics link.

Fig.1 shows the schematic diagram of microwave arbitrary waveforms. A beam of light from the tunable laser source (TLS) enters a Sagnac loop via a polarization controller (PC). In the Sagnac loop[18,19], the light is split by a polarization beam splitter (PBS) into two orthogonally polarized light waves which travel along with the clockwise and counter-clockwise directions respectively, and

* This work has been supported by the National Natural Science Foundation of China (No.61875070), the Science and Technology Development Plan of Jilin Province (Nos.20160519010JH, 20170204006GX and 20180201032GX), and the Science and Technology Project of Education Department of Jilin Province (No.JJKH20190110KJ).

** E-mail: dongw@jlu.edu.cn

then they are merged in a polarization modulator (PolM). As shown in Fig.1, the clockwise and counter-clockwise light are injected into PolM, which are driven by an RF signal with frequency of f_m. Due to the principle of velocity match, the clockwise light can be modulated effectively in Fig.2(b). Thus, the optical carrier with frequency of f_0 and six sidebands with a frequency interval of f_m are existed in optical spectrum. However, along the counter-clockwise direction, light waves and microwaves travel in the opposite direction, which could result in a weak modulation as shown in Fig.2(a). In weak modulation, the optical spectrum has only the optical carrier with frequency of f_0. As a result, a modulated optical signal meets an unmodulated signal in PBS. It is noted that even-order sidebands suppressed signals can be obtained after polarizer (Pol) by adjusting PCs (PC3 and PC4) and PolM, which is equivalent to introducing a static phase shift to the modulation signal. At the output of PBS, optical signals consisting of ±1st-order and ±3rd-order sidebands are generated as shown in Fig.2(c). We could find the odd-order sidebands are combined with the counterclockwise propagated optical carrier at the Pol. Meanwhile, the lower part is modulated by an RF signal of which the frequency is f_p. By setting the bias of the MZM, a modulated light wave with only odd-order sidebands is obtained and sent into a single mode fiber (SMF) as pump light. Subsequently, the unwanted optical sidebands are filtered out by the SBS effect, leaving only the carrier, the +1st-order, and the +3rd-order sidebands. Ultimately, a triangular wave, a square wave and a sawtooth waveform can be generated after PD by adjusting the modulation index and phase.

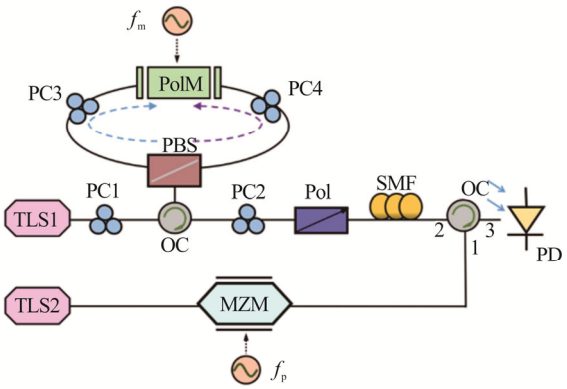

TLS: tunable laser source; OC: optical circulator; PC: polarization controller; PBS: polarization beam splitter; PolM: polarization modulator; Pol: polarizer; MZM: Mach-Zehnder modulator; PD: photodetector; SMF: single mode fiber; Black solid line: optical path; Black dotted line: electrical path

Fig.1 Schematic diagram of the arbitrary wave signal generator

In the mathematical expression, the clockwise light field can be written as:

$$E_{\text{PBS-cw}} = E_{\text{cw}}\exp(\text{j}wt)\sum_{k=1}^{\infty} J_{\text{k}}(\beta)\times \left\{\exp\left[\text{j}k\omega_{\text{m}}t\right]-\exp\left[-\text{j}k\omega_{\text{m}}t\right]\right\}, \quad (1)$$

where $E_{\text{cw}}=E_0\cos\theta$ is the amplitude of the electrical field of the clockwise propagation light wave. Assuming that the amplitude of the electrical filed of the CW light wave from the TLS1 is E_0, and the polarization direction of the incident light from the TLS1 is aligned at an angle of θ relative to one principal axis of the PBS, β is the phase modulation index, $\omega_0=2\pi f_0$ and $\omega_{\text{m}}=2\pi f_{\text{m}}$ are the angular frequency of the optical carrier and the modulated microwave signal respectively, $J_k(\cdot)$ denotes the kth-order of the first kind of Bessel function[20]. After combining the counter-clockwise modulation signal with the clockwise optical signal, the PC is adjusted to form an angle of α with the principle axis of PBS, and the output light field can be expressed as

$$E_{\text{pol}}=E_{\text{PBS-cw}}\cos\alpha+E_{\text{PBS-cw}}\sin\alpha. \quad (2)$$

Here, the counter-clockwise light can be written as:

$$E_{\text{PBS-ccw}}=E_0\exp(\text{j}\omega t)\sin\theta. \quad (3)$$

Assuming that $\theta=\alpha=45°$, the PC and the PolM are adjusted to suppress the even order sidebands, and the output optical signal of the Pol can be expressed as

$$E_{\text{pol}} = \frac{1}{2}E_0\exp(\text{j}2\pi f_0 t)\{1+ J_1(\beta)[\exp(\text{j}2\pi f_{\text{m}}t)-\exp(-\text{j}2\pi f_{\text{m}}t)]+ J_3(\beta)[\exp(\text{j}6\pi f_{\text{m}}t)-\exp(-\text{j}6\pi f_{\text{m}}t)]+\ldots\}. \quad (4)$$

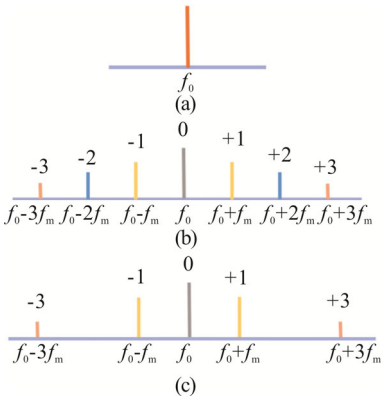

Fig.2 Spectra modulated after (a) modulating in the Sagnac loop, (b) passing through PolM, and (c) adjusting the PC3 and PC4

After the light in the lower branch passing through MZM, the bias voltage of MZM is adjusted to obtain ±1st-order sidebands, which are sent to SMF as pump light to generate the SBS effect. In general, the Brillouin frequency shift can be approximately expressed as

$$v_{\text{B}}= 2nv_{\text{A}}/\lambda_{\text{P}}\ , \quad (5)$$

where n represents the effective refractive index of the fiber, v_{A} represents the velocity of the acoustic wave, and λ_{P} represents the wavelength of the pump wave. In general, the Brillouin gain spectrum $g(f)$ and loss spectrum $\alpha(f)$ generated by the SBS effect can be given by

$$g(f)=\frac{g_0}{2}\frac{(\Delta v_{\text{B}}/2)^2}{f^2+(\Delta v_{\text{B}}/2)^2}+\text{j}\frac{g_0}{4}\frac{\Delta v_{\text{B}}f}{f^2+(\Delta v_{\text{B}}/2)^2}\ , \quad (6)$$

$$\alpha(f)=-\frac{g_0}{2}\frac{(\Delta\nu_B/2)^2}{f^2+(\Delta\nu_B/2)^2}-\mathrm{j}\frac{g_0}{4}\frac{\Delta\nu_B f}{f^2+(\Delta\nu_B/2)^2}\quad,(7)$$

where $g_0=g_B I_P L_{eff}/A_{eff}$, g_B denotes line center gain coefficient and I_P denotes the power of the pump light, L_{eff} represents effective fiber length, A_{eff} represents effective mode area, ν_B is Brillouin frequency shift, $\Delta\nu_B$ is Brillouin linewidth, and f is the frequency offset from the gain and loss spectrum center.

The lower part of the optical signal from TLS2 is transmitted into the MZM, which is modulated by an RF signal at f_p. By setting the bias of the MZM, the optical sidebands at f_c+f_p and f_c-f_p are obtained and sent into SMF as pump light, as shown in Fig.3(b). Meanwhile, the previous modulated light is injected into the same SMF in the opposite direction. Then the SBS process of the modulated signal is performed[21,22], and −1st-order sideband and −3rd-order sideband can be suppressed completely as illustrated schematically in Fig.3(c). Therefore, the optical field of a single sideband modulation signal composed of −1st-order sideband and −3rd-sideband can be expressed as

$$\begin{aligned}E_{pol}=&\frac{1}{2}E_0\exp(\mathrm{j}2\pi f_0 t)+\frac{1}{2}E_0\exp(\mathrm{j}2\pi f_0 t)\times\\&\{J_1(\beta)[\exp(\mathrm{j}2\pi f_m t)-\alpha[(f_{p1}+\nu_B)-\\&(f_0+f_m)]\exp(-\mathrm{j}2\pi f_m t)]+\\&J_3(\beta)[\exp(\mathrm{j}6\pi f_m t)-\alpha[(f_{p2}+\nu_B)-\\&(f_0+f_m)]\exp(-\mathrm{j}6\pi f_m t)\},\end{aligned}\quad(8)$$

where $f_{p1}=f_{c1}+f_p$ and $f_{p2}=f_{c1}-f_p$. After PD, the output electrical signal can be expressed as

$$\begin{aligned}I(t)=&R\{\frac{1}{4}E_0^2+\frac{1}{4}E_0^2J_1^2(A^2+1)+\frac{1}{4}E_0^2J_3^2(A^2+1)+\\&\frac{1}{2}E_0^2J_1[\cos(2\pi f_m t)-\cos(\varphi_a+2\pi f_m t)]+\\&\frac{1}{2}E_0^2J_3[\cos(6\pi f_m t)-A\cos(\varphi_a+\mathrm{j}6\pi f_m t)]+\\&E_0^2J_1J_3\cos[A^2\cos(4\pi f_m t)-A\cos(\varphi_a+8\pi f_m t)]-\\&\frac{1}{2}AE_0^2J_1^2\cos(\varphi_a+4\pi f_m t)-\\&\frac{1}{2}AE_0^2J_3^2\cos(\varphi_a+12\pi f_m t)\}.\end{aligned}\quad(9)$$

And the four parameters are given by the following equations:

$$G=\exp\{\frac{g_0}{2}\frac{(\frac{\Delta\nu_B}{2})^2}{(f_{p1}-\nu_B-f_0+f_c)^2+(\frac{\Delta\nu_B}{2})^2}\}\quad,\quad(10)$$

$$A=\exp\{-\frac{g_0}{2}\frac{(\frac{\Delta\nu_B}{2})^2}{(f_{p2}-\nu_B-f_0+f_m)^2+(\frac{\Delta\nu_B}{2})^2}\}\quad,\quad(11)$$

$$\varphi_g=\frac{g_0}{4}\frac{\Delta\nu_B(f_{p1}-\nu_B-f_0+f_m)}{(f_{p1}-\nu_B-f_0+f_m)^2+(\frac{\Delta\nu_B}{2})^2}\quad,\quad(12)$$

$$\varphi_a=-\frac{g_0}{4}\frac{\Delta\nu_B(f_{p2}-\nu_B-f_0+f_m)}{(f_{p2}-\nu_B-f_0+f_m)^2+(\frac{\Delta\nu_B}{2})^2}\quad,\quad(13)$$

and R is the responsivity to PD.

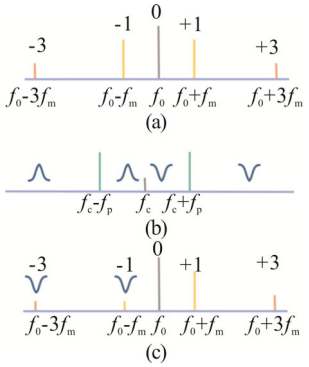

Fig.3 The schematic diagram of the SBS effect process: (a) The output spectrum of the upper branch; (b) The output spectrum of the lower branch; (c) The output spectrum of the SBS effect

In Eq.(9), the first three DC components can be easily removed by using DC block equipment in the experiment; therefore, Eq.(9) can be simplified as follows:

$$\begin{aligned}I(t)\approx&\frac{1}{2}R\{\frac{1}{2}E_0^2J_1[\cos(2\pi f_m t)-A\cos(\varphi_a+2\pi f_m t)]+\\&\frac{1}{2}E_0^2J_3[\cos(6\pi f_m t)-A\cos(\varphi_a+6\pi f_m t)]+\\&E_0^2J_1J_3\cos[A^2(4\pi f_m t)-A\cos(\varphi_a+8\pi f_m t)]-\\&\frac{1}{2}AE_0^2J_1\cos(\varphi_a+4\pi f_m t)-\frac{1}{2}AE_0^2J_3^2\cos(\varphi_a+12\pi f_m t)\}\end{aligned}.\quad(14)$$

Because the stimulated Brillouin loss is relatively high in the experiment, and the SBS induced nonlinear phase shift φ_a is calculated to be zero, so the components with coefficients A and A^2 can be ignored. Therefore, Eq.(14) can be simplified as follows:

$$I(t)=\frac{1}{4}E_0^2R\{J_1\cos(2\pi f_m t)+J_3\cos(6\pi f_m t)\}\quad.\quad(15)$$

Based on the theoretical diagram shown in Fig.1, the simulation is carried out. A beam of polarized[18] light from TLS1 at 1 550.33 nm is injected into the Sagnac loop through PC1. The RF signal at 10 GHz was applied to the PolM, the power of the RF signal is controlled to 16 dBm, the half-wave voltage of PolM is 3.3 V, and the microwave transmission loss is 2 dB. Two quadratically polarized lights travel clockwise and counterclockwise through the PolM in the Sagnac loop. Because of the velocity mismatch, unmodulated and modulated optical signals are generated in opposite propagation direction. Then by adjusting PC3 and PC4, even sidebands can be effectively suppressed at the output of PBS, and the optical carrier and ±1st-order and ±3rd-order sidebands remain unchanged. Meanwhile, a beam of light from TLS2 at 1 550.58 nm is emitted into the MZM, which is modulated by the RF signal at 10 GHz to produce the

±1st-order sidebands with the suppressed carrier. The output power of TLS1 and TLS2 is about 10 dBm, and the power of RF signal at f_p is 16 dBm. The ±1st-order sidebands are used as pump light to generate the SBS effect. Ultimately, the optical signal is applied to PD to generate a triangular waveform with a variable repetition frequency equal to the frequency of the RF signal applied to the MZM.

The Fourier series expansion of a typical triangular waveform sequence $Q_{tr}(t)$ is given by[23]

$$Q_{tr}(t) = C_{tr} + D_{tr} \sum_{k=1,3,5}^{\infty} \frac{1}{k^2} * \cos(k\omega t) \quad , \tag{16}$$

where C_{tr} and D_{tr} are two DC constants. According to Eq.(16), a triangular waveform only has odd-order harmonics. Fig.4(a) shows the waveform output from the Pol. As can be seen from Eq.(15) an ideal triangular waveform having two components are obtained when the modulation index β is set to 1.51, which is shown in Fig.4(c). The root-mean square error (*RMSE*) can be calculated as

$$RSME = \sqrt{\frac{1}{n}\sum (I_0 - I_1)^2} \quad , \tag{17}$$

where I_0 is the ideal triangular Fourier series, and I_1 is the triangular waveform generated in the proposed system. Comparing with the standard triangular wave in Fig.4(b), the *RMSE* is 0.005 5, which is far less than the theoretical value[24] and close to the ideal value.

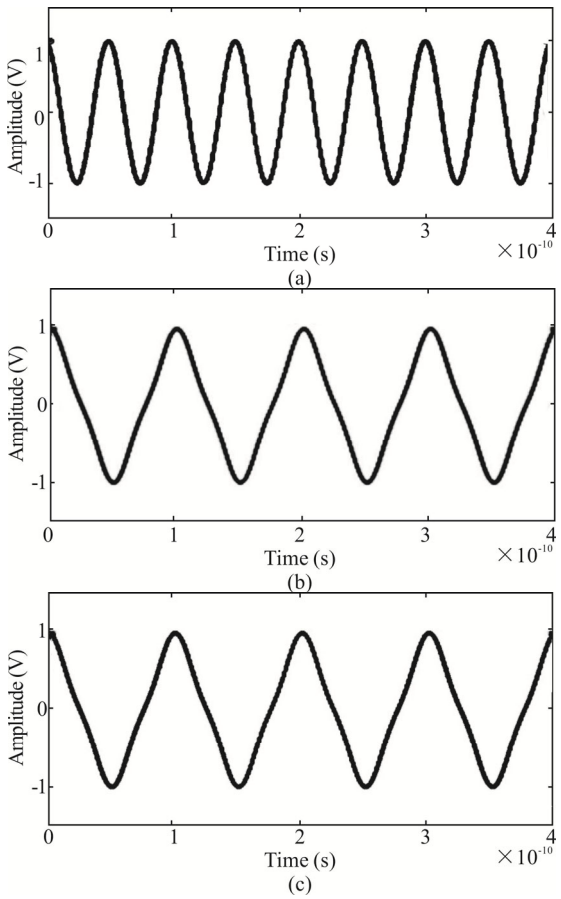

Fig.4 (a) The wave diagram without the SBS effect measured in simulation; (b) Standard triangular wave diagram measured in simulation; (c) The triangular wave diagram of Fig.1 in the simulation

By changing the frequency of the modulated RF signal, the repetition rate of the obtained triangular waveform can be changed to 20 GHz or 40 GHz as shown in Fig.5.

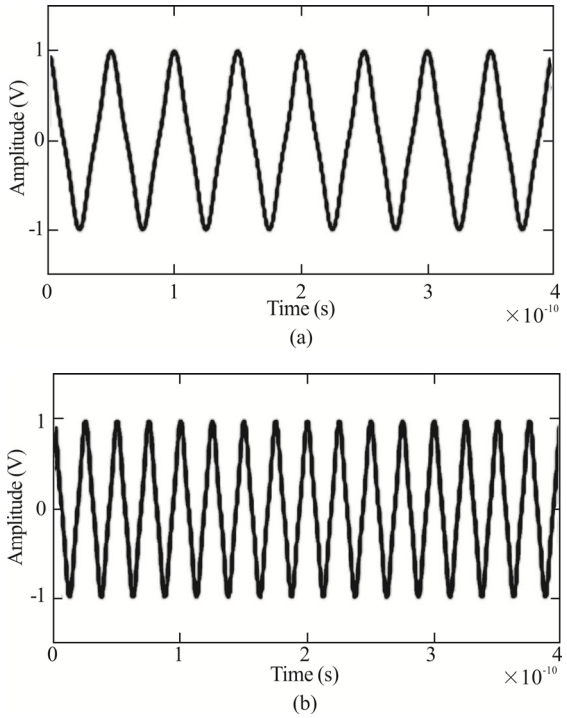

Fig.5 Triangular wave simulation diagrams with a repetition rate of (a) 20 GHz and (b) 40 GHz

The Fourier series expansion of a typical square waveform sequence $Q_{sq}(t)$ is given by

$$Q_{sq}(t) = C_{sq} + D_{sq} \sum_{k=1,3,5}^{\infty} \frac{1}{k} * \sin(k\omega t) \quad , \tag{18}$$

where C_{sq} and D_{sq} are two DC constants. Comparing the expression of $I(t)$ in Eq.(15) with the Fourier series expansion of a square waveform sequence $Q_{sq}(t)$ in Eq.(18), the square waveform generation is similar to the triangular waveform generation. In order to generate an ideal square waveform, the modulation index should be set as 6.10. After changing the input signals with different frequencies, the square waveforms with different repetition rates can be obtained as depicted in Fig.6.

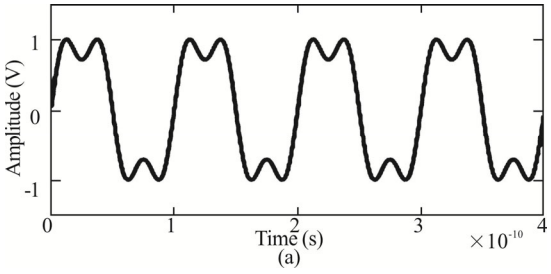

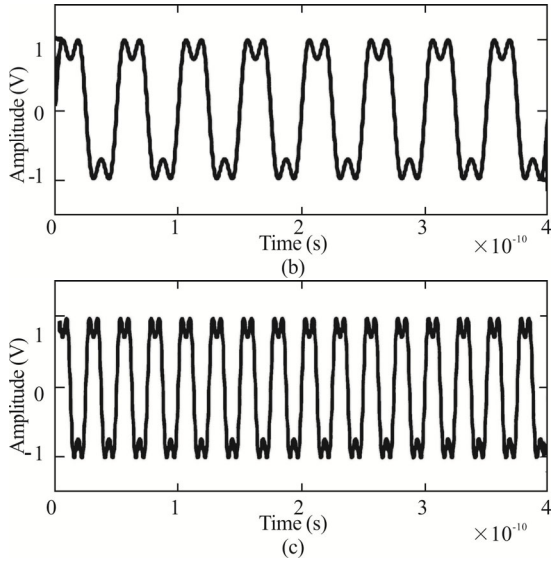

Fig.6 Square waveform simulation diagrams with a repetition rate of (a) 10 GHz, (b) 20 GHz, and (c) 40 GHz

The Fourier series expansion of a typical sawtooth waveform sequence $Q_{sw}(t)$ is given by

$$Q_{sw}(t) = C_{sw} + D_{sw}\sum_{k=1}^{\infty}\frac{1}{k} * \sin(k\omega t) \quad , \tag{19}$$

where C_{sw} and D_{sw} are two DC constants. As can be seen from Eq.(19), the sawtooth waveform has odd-order and even-order harmonics, and a sawtooth waveform generation is similar to the generation of the square waveform. However, it should be ensured that the following relationship is established to obtain an ideal sawtooth wave[25]

$$\frac{J_2(\beta)}{J_1(\beta)} = \frac{\sin(\varphi/2)}{2\cos(\varphi/2)} \quad , \tag{20}$$

$$\frac{J_3(\beta)}{J_1(\beta)} = -\frac{1}{3} \quad . \tag{21}$$

In this case, the static phase should be 0.35π, which can be implemented by tuning PC3 and changing the power of the RF signal. In consequence, the attained sawtooth waveform is shown in Fig.7.

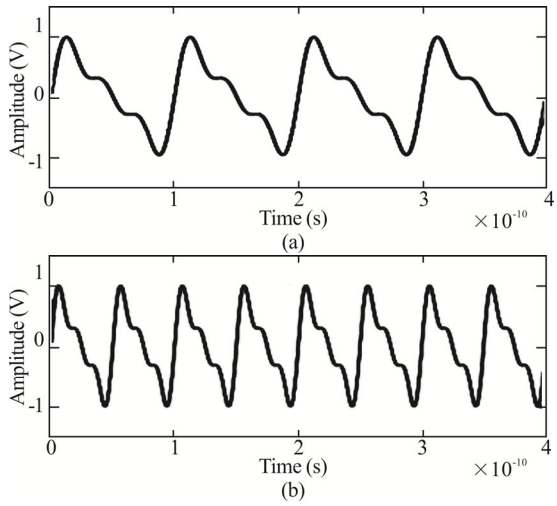

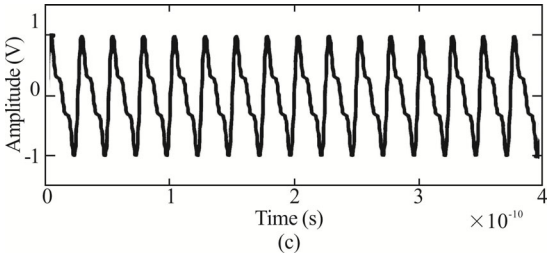

Fig.7 Sawtooth waveform simulation diagrams with a repetition rate of (a) 10 GHz, (b) 20 GHz, and (c) 40 GHz

In conclusion, we propose and demonstrate a new scheme for generating arbitrary waveform microwave waveforms based on the Sagnac loop and SBS effect. The key technique in Sagnac loop is that the counter-clockwise light is not modulated, while the clockwise light is effectively modulated. Once the frequency of the modulated microwave signal is changed, the arbitrary microwave waveform signals with variable repetition rate will be obtained. The system has full optical potential. The stability of the system has been improved with the help of Sagnac loop. Thus, this scheme is particularly attractive as a waveform generation source for radar systems and photonic network applications.

References

[1] Yao J, Optics Communications **284**, 3723 (2011).

[2] R. S. Bhamber, A. I. Latkin, S. Boscolo and S. K. Turitsyn, All-optical TDM to WDM Signal Conversion and Partial Regeneration Using XPM with Triangular Pulses, Proc. 34th Eur. Conf. Opt. Commun., Brussels, Belgium, 1 (2008).

[3] Mckinney J D, Leaird D E and Weiner A M, Optics Letters **27**, 1345 (2002).

[4] Khan M H, Shen H, Xuan Y, Zhao L, Xiao S, Leaird D E, Weiner A M and Qi M, Nature Photonics **4**, 117 (2010).

[5] Leaird D E and Weiner A M, Optics Letters **29**, 1551 (2004).

[6] Wu R, Supradeepa V R, Long C M, Leaird D E and Weiner A M, Optics Letters **35**, 3234 (2010).

[7] Wang C and Yao J, Journal of Lightwave Technology **28**, 1652 (2010).

[8] Jiang Y, Ma C, Bai G, Qi X, Tang Y, Jia Z, Zi Y, Huang F and Wu T, Optics Express **23**, 19442 (2015).

[9] Zhang J and Yao J, Journal of Lightwave Technology **34**, 5610 (2016).

[10] Guang-Fu Bai, Lin Hu, Yang Jiang, Jing Tian, Yue-Jiao Zi, Ting-Wei Wu and Feng-Qin Huang, Optics Communications **396**, 134 (2017).

[11] Yuan J, Ning T, Li J, Pei L, Zheng J and Li Y, Scientific Reports **8**, 3369 (2018).

[12] He H, Shao L Y, Wang C, Luo B, Zou X, Zhang X, Pan W and Yan L, IEEE Photonics Technology Letters **30**, 943 (2018).

[13] Zhang K, Zhao S, Li X, Lin T and Wang G, Optics Communications **453**, 124326 (2019).
[14] Liu W, Wang M and Yao J, Journal of Lightwave Technology **31**, 1636 (2013).
[15] Gao Y, Wen A, Liu L, Tian S, Xiang S and Wang Y, Journal of Lightwave Technology **33**, 2899 (2015).
[16] Chandra S, Vardhanan A V and Gangopadhyay R, Iet Circuits Devices & Systems **2**, 123 (2008).
[17] Liu X, Pan W, Zou X, Zheng D, Yan L, Luo B and Lu B, Journal of Lightwave Technology **32**, 3797 (2014).
[18] W. Liu and J. Yao, Journal of Lightwave Technology **32**, 3637 (2014).
[19] Li W, Wang WY, Wang WT, Liu JG and Zhu NH, IEEE Photonics Journal **6**, 1 (2014).
[20] Wang D, Tang X, Xi L, Zhang X and Fan Y, Optics & Laser Technology **116**, 7 (2019).
[21] Du C, Wang Y, Wang D, Li Q, Sun X, Dong W and Zhang Xindong, Optical and Quantum Electronics **51**, 25 (2019).
[22] Xiao Yongchuan, Guo Jing, Wu Kui, Dong Wei and Qu Pengfei, Optics Express **21**, 31740 (2013).
[23] V. Torres-Company, J. Lancis, P.Andr´es and L. R. Chen, Journal of Lightwave Technology **26**, 2476 (2008).
[24] Zhai W, Wen A and Shan D, Journal of Lightwave Technology **37**, 1 (2019).
[25] Zhu S, Li M and Wang X, Optics Letters **44**, 94 (2019).